Optimized MIMO Feeder Link Architectures for 6G NGSO Mega-Constellations

Oscar Martinez, Thomas Delamotte, Andreas Knopp

Chair of Signal Processing
University of the Bundeswehr Munich
Neubiberg, Germany
papers.sp@unibw.de

Abstract—Multiple antenna feeder links are a promising solution to address the forecasted data-rate bottlenecks in future 6G Non-Geostationary Orbit (NGSO) constellations. In this paper, a comparative analysis of feeder architectures is conducted between the Uniform Linear Array (ULA) and the Uniform Circular Array (UCA). The study starts with a NGSO trajectories examination, followed by the derivation of the instantaneous optimal capacity conditions. Furthermore, a novel key performance indicator based on the inverse condition number of the channel matrix is introduced. This indicator facilitates performance comparison across the Field-of-View (FoV). Numerical simulations evaluating array orientation dependence, orbit altitude influence, and frequency stability, indicate better performance for ULA geometries, thus positioning them as a suitable choice to scale the system throughput.

Index Terms—NGSO feeder link, Uniform Linear Array, Uniform Circular Array, LoS MIMO, Inverted Condition Number.

I. INTRODUCTION

Low Earth Orbit (LEO) mega-constellations are emerging as a potential solution to achieve the 6G goal of providing broadband internet access worldwide. The interest of these orbits is shorter transmission distances, compared to traditional GEO (geostationary orbit) systems, which yield up to a 20-fold reduction in latency and a 30 dB path loss reduction in the typically used Ka-band.

However, LEO satellites, due to their proximity to the Earth's surface, have limited coverage, thus requiring a vast network of ground stations (GSs) across the globe to guarantee continuous feeder link access. Typically, GS deployments are costly. They entail strategically locating the antennas to ensure they meet the required traffic demand, visibility, favorable weather conditions, low interference, and a direct connection to the backbone network. While advancements in Inter-Satellite Links (ISL) technology are yielding results and reducing the required number of GSs, the remaining gateways must scale up their capacity to serve more users [1], [2].

Furthermore, NGSO feeder link bottleneck is becoming evident with the rapid increase in NGSO-internet subscribers. A clear example of performance degradation due to congestion

is the Starlink experience in North America during 2022. In particular, uplink limitations may have led to important service quality degradation, despite the large number of Starlink GSs already deployed in the region [3]. This situation is expected to worsen, especially with Starlink expansion projects, aiming to increase the number of satellites by a factor of 7. The challenge now is to maximize the total throughput that a gateway area can provide. To achieve this, Line-of-Sight (LoS) Multiple-Input Multiple-Output (MIMO) solutions have already been proposed for satellite networks, for example in [4]–[9].

Currently, LEO ground station technology consists of up to 40 high-gain fully steerable dish antennas per site, as indicated by the FCC filing of Starlink [10]. However, only a part of the ground antennas establish connections with visible satellites. In fact, a single ground antenna per satellite is utilized. Meanwhile, the remaining antennas only serve as backup hardware. In contrast, in the MIMO paradigm, the transmission of the GS is coordinated among several antennas, targeting the orbiting satellites collectively as illustrated in Fig. 1. This concept has been explored and proven effective in geostationary communication in [4]–[6]. More recently, this technology has been proposed for LEO constellations in [7]–[9].

Beyond GSs geographic location problem, NGSO mega-constellations research has investigated challenges arising from the traveling speed of satellites, notably Doppler shift and rapid antenna tracking. Nevertheless, the scaling of the feeder link capacity remains pending. This paper aims to shed light on the optimization of architecture for MIMO GS's topologies.

The paper is structured as follows. First, the channel model and capacity bounds are presented alongside an abstraction for constellations dynamics in Section II. Afterwards, the array geometries are described in Section III. The proposed comparison methodology is explained in Section IV, before analyzing the numerical results and design trade-offs in Section V. Finally, the concluding remarks are provided in Section VI.

II. SYSTEM CHARACTERISATION

A. Uplink MIMO Feeder Link Channel Model

The scenario under consideration consists of several directive antennas installed on a LEO satellite, with their beams pointed towards a group of cooperative gateways on ground

as depicted in Figure 1. Given the focus solely on comparing ground array distributions, clear sky conditions are assumed. Moreover, LEO Doppler shift compensation has been extensively studied for decades, with established solutions for LEO MIMO architectures [11]. Therefore, perfect Doppler compensation is assumed in the model. Similarly, MIMO feeder link phase and time synchronization over fiber have shown optimal results for distances up to tens of kilometers [12]. Consequently, synchronization inaccuracies are considered to be negligible.
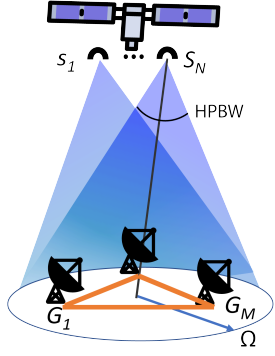

Fig. 1: Graphic representation of MIMO with a single platform

In this context, the MIMO feeder link model for uplink [1] is characterized by a Line-of-Sight channel matrix $\mathbf{H} \in \mathbb{C}^{N \times M}$ with N and M the number of space and ground antennas, respectively. The (n, m)-entry of the matrix is given by:

$$h_{n,m} = a_{n,m} e^{-j\frac{2\pi f_c}{c_0} r_{n,m}}. \tag{1}$$

The first factor corresponds to the signal complex envelope $a_{n,m}$. it is calculated as $a_{n,m} = \frac{c_0 e^{j\varphi_0}}{4\pi f_c r_{n,m}}$, with c_0 the speed of light in free space, $r_{m,n}$ the distance between each pair of antennas, and φ_0 a common phase, taken to be zero with no loss of generality. Furthermore, since all ground antennas are illuminated by the all of the payload beams, the GS array size is bounded by the beam intersection surface (Ω). The site's field of view is comprised between the geocentric angle $\beta \in [0, \beta_{max}]$ as shown in Fig. 2.

The distance $r_{n,m}$ within the envelope $a_{n,m}$, is effectively approximated by considering an identical observation angle β_0 for all pair of ground and on-board antennas. β_0, represents the geocentric angle between the ground and space array centers. Therefore, $r_{n,m}$ is expressed as:

$$r_{n,m} \approx \hat{r}(\beta_0) = \sqrt{R_e^2 + R_s - 2R_e R_s \cos\beta_0}, \tag{2}$$

where R_e and R_s are the mean Earth and the orbit radius, respectively. Using this simplification, $a_{n,m}$ becomes $a_{n,m} \approx a(\beta_0) = \frac{c_0}{4\pi f_c \hat{r}_0(\beta_0)}$. It is important to note that this approximation is not applicable to the phase component of H. Expressions for the exponential term in each array scenario are calculated later in Section III.

[1]Downlink MIMO model is equivalent, but N representing the number of ground antennas and M the number of space antennas
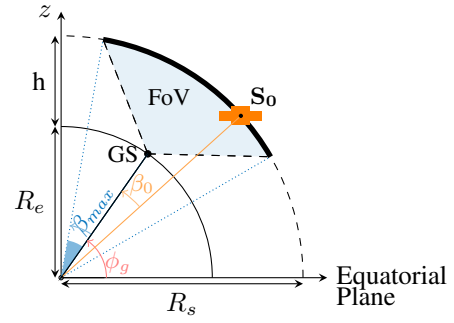

Fig. 2: 2D representation of the GS field-of-view and the geocentric angle β

B. *Los MIMO Spectral Efficiency*

The MIMO capacity is a function of the $\mathbf{H}$ matrix properties and the carrier-to-noise ratio (CNR) as found in [13]:

$$C = \log_2\left[\det(\mathbf{I_N} + \rho \cdot \mathbf{V})\right], \tag{3}$$

with ρ calculated as $\rho = \frac{P_{TX} \cdot g_{TX} \cdot g_{RX}}{kT}$, is accounting for the CNR, P_{TX} represents the transmit power, and g_{TX} and g_{RX} are the linear gains of the transmitting and receiving antennas, respectively. kT denotes the system noise power at the receiving end, with T the noise temperature and k the Boltzmann constant. It is worth mentioning that ρ does not include the path-loss, which is already comprised in $\mathbf{V}$.

$$\mathbf{V} = \begin{cases} \mathbf{HH}^H & N < M \\ \mathbf{H}^H\mathbf{H} & N \geq M \end{cases}. \tag{4}$$

Authors in [4] demonstrated that in general, the spectral efficiency of a LoS MIMO system can be expressed as non-interfering single-input-single-output (SISO) channels. Let $\mathcal{M}_{max} = \max\{M, N\}$ and $\mathcal{M}_{min} = \min\{M, N\}$. The system capacity is then rewritten as:

$$C = \sum_{i=1}^{\mathcal{M}_{min}} \log_2(1 + \rho\gamma_i), \tag{5}$$

with γ_i the eigenvalues of the $\mathbf{V}$ matrix and $\rho\gamma_i$, the CNR of the equivalent SISO channel. The upper bound for the capacity is found for $\gamma_i = \gamma_{opt} = |a(\beta_0)|^2 \mathcal{M}_{max}$. The instantaneous optimum capacity, explicitly considering the dependence on the observation angle (β_0) is expressed as follows:

$$C_{opt}(\beta_0) = \mathcal{M}_{min} \log_2(1 + \rho|a(\beta_0)|^2\mathcal{M}_{max}). \tag{6}$$

In contrast, the lower bound of the capacity or *keyhole*, appears when there is only one non-zero eigenvalue $\gamma_{key} = |a(\beta_0)|^2 \mathcal{M}_{max}\mathcal{M}_{min}$. The keyhole capacity is then:

$$C_{key}(\beta_0) = \log_2(1 + \rho|a(\beta_0)|^2\mathcal{M}_{max}\mathcal{M}_{min}). \tag{7}$$

With the understanding the eigenvalues' impact on the link performance, the objective is now to analyze and compare their quality across the entire FoV. The performance indicator accounting this is detailed in Section IV.

C. NGSO constellation motion

In this subsection, we present an abstraction for the dynamics of mega-constellations necessary for understanding LoS MIMO performances. For the sake of simplicity, the model uses a spherical representation of the Earth, circular orbits and two main parameters to summarize the configuration :

- Semi-major axis (R_s): Orbital radius measured from the center of the Earth. For the abstraction, R_s is constant and equal to the sum of the mean Earth radius and the altitude (h) (ranging from 160 to 2500 km in LEO).
- Inclination angle (ϑ): Angle between the orbital planes and the equator.

We consider here, a single shell constellation, i.e. a satellites orbiting at the same altitude and inclination. However, our study will also provide insights for the multi-shell scenarios.

The latitude ϕ and longitude λ of a sub-satellite point (SSP) are given by:

$$\sin(\phi) = \sin\vartheta \sin\nu, \tag{8}$$

$$\lambda = \arctan 2\left(\cos\vartheta \sin\nu, \cos\nu\right) + \lambda_0 - \frac{\omega_e}{\omega_s}\nu. \tag{9}$$

Here, ν represents the true anomaly, which describes the satellite's progress in the orbit and ranges between $(-\pi, \pi]$. λ_0 is the satellite's longitude offset, while ω_e and ω_s denote the angular velocities of the Earth and the satellite respectively. The trajectory can then be divided into two sections based on the satellite's direction: ascending towards the northern hemisphere or descending towards the southern hemisphere, as depicted in Fig. 3a. The two sections form a regular grid over the gateway site's field-of-view, as shown in Fig. 3b. This indicated that the optimal MIMO architecture should maximize the capacity for both complementary segments simultaneously.

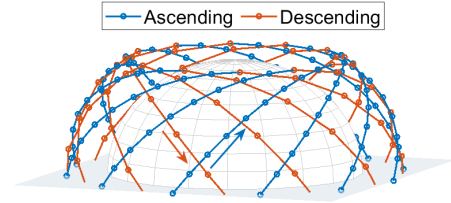## III. MATHEMATICAL DESCRIPTION FOR THE ARRAY GEOMETRIES

In this section, we present the mathematical representation for the two array types under study. This mathematical description has already been provided in [4], [14] for the GEO context. Therefore, our focus is only on incorporating the changes related to the satellite motion.

A. Uniform Linear Array (ULA)

The elements positions are given by their distance d_m to the center of the array and a common tilt angle δ_g with respect to the East-West tangent line as depicted in Fig. 4a. The m-th element coordinates in Earth-Centered, Earth-Fixed (ECEF) reference are $(x_m, y_m, z_m)^T = \mathbf{G_0} + \mathbf{p_m}$, starting from the site's origin ($\mathbf{G_0}$) plus a position vector $\mathbf{p_m}$ [4].

$\mathbf{G_0} = R_e(\cos\lambda_0 \cos\phi_0, \cos\phi_0 \sin\lambda_0, \sin\phi_0)^T$ and $\mathbf{p_m}$ is calculated as:

$$\mathbf{p_m} = d_m \cdot \begin{pmatrix} -\sin\lambda_0 \cos\delta_g - \sin\phi_0 \cos\lambda_0 \sin\delta_g \\ \cos\lambda_0 \cos\delta_g - \sin\phi_0 \sin\lambda_0 \sin\delta_g \\ \cos\lambda_0 \sin\delta_g \end{pmatrix}. \tag{10}$$

(a) Ascending and descending segments, 70° inclination
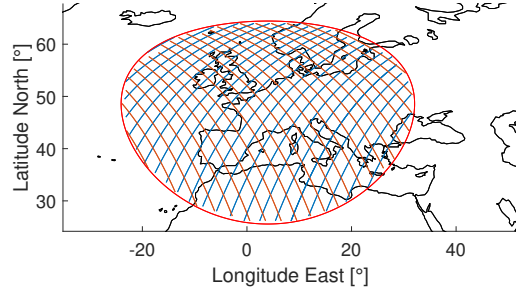
(b) SSP grid in the Field of view centered at (45°N, 4°E)

Fig. 3: Constellation behavior
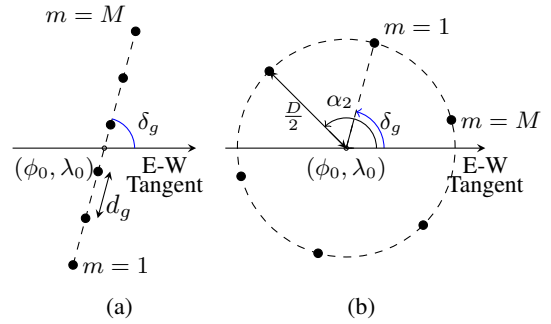

(a)   (b)

Fig. 4: Graphical description of the arrays geometry, ULA (a) and UCA (b).

with $d_m = d_g \cdot \left(m - \frac{M+1}{2}\right)$ the distance to the ULA center.

B. Uniform Circular Array (UCA)

Similarly to ULAs, UCA elements are parameterized by their angle from the reference tangent East-West direction ($\boldsymbol{\alpha}_m$), and a common distance to the center $D/2$. The graphical representation of the UCA is shown in Fig. 4b. Given an offset angle δ_g, the angle $\boldsymbol{\alpha}_m$ is as follows:

$$\boldsymbol{\alpha}_m = \frac{2\pi}{M}(m-1) + \delta_g. \tag{11}$$

Then, as for the ULA, the coordinates of the elements consist of the center of the array and a position vector:

$$E_m = \mathbf{G_0} + \frac{D}{2}\begin{pmatrix} -\sin\lambda_0 \cos\alpha_m - \sin\phi_0 \cos\lambda_0 \sin\alpha_m \\ \cos\lambda_0 \cos\alpha_m - \sin\phi_0 \sin\lambda_0 \sin\alpha_m \\ \cos\lambda_0 \sin\alpha_m \end{pmatrix}. \tag{12}$$

C. Instantaneous Optimal Capacity

As already stated, our investigation focuses on the Fig. 1 scenario, where the space antennas are installed on the same platform. Consequently, due to dimensional, weight, and power constrains of the satellite, we have opted to consider only two space antennas. The coordinates of the resulting two-element ULA for orbiting array are described with the center $\mathbf{S_0}$ and position vector $\mathbf{s_n}$, using (10). The corresponding parameters are then $\phi_s, \lambda_s, \delta_s, d_s$.

The MIMO $2 \times M$ achieves C_{opt} (6), int the case of the ULA array when [4]:

$$(r_{1,k} - r_{2,k}) - (r_{1,l} - r_{2,l}) = \zeta(k-l)\frac{c_0}{Mf_c}. \quad (13)$$

The instantaneous optimum capacity condition for the UCA is equivalent, with the term $(k-l)$ replaced by the operator $\ominus$, as defined in [14]:

$$k \ominus l \triangleq \begin{cases} k-l & |k-l| \leq \frac{M}{2} \\ k-l - M \cdot \text{sign}(k-l) & |k-l| > \frac{M}{2} \end{cases}. \quad (14)$$

Here, f_c is the channel frequency, with $k,l = 1,...,M$, and $\zeta \in \mathbb{Z}$, an integer not divisible by M.

Unlike the GEO scenario, the distance $r_{n,m}$ between antennas is also dependent on the instantaneous position of the satellite (ϕ_s, λ_s) and the relative orientation of the space array. This dependence turn the channel optimization infeasible for the entire FoV (with fixed arrays dimensions) as it is demonstrated below.

First, the value of $r_{n,m} = ||(\mathbf{S_0} + \mathbf{s_n}) - (\mathbf{G_0} + \mathbf{g_m})||$ is expressed for the ULA as:

$$r_{n,m}^2 = s_n^2 - p_m(c_n + 2d_s \cos \Delta\delta) - p_m^2, \quad (15)$$

$\Delta\delta = \delta_g - \delta_s$ is the relative angle between the two arrays, and for the UCA:

$$r_{n,m}^2 = s_n^2 + \frac{D}{2}c_{n,m} + \frac{D^2}{4}. \quad (16)$$

In both cases, the term s_n represents the distance from the center of the land array to the n-th satellite antenna $s_n = \sqrt{R_s^2 + R_e^2 - 2R_S R_e \cos(\beta_{0,n})}$, with $\beta_{0,n}$ the geocentric angle, calculated as

$$\cos \beta_{0,n} = \cos \phi_n \cos \phi_0 \cos \Delta\lambda + \sin \phi_n \sin \phi_0. \quad (17)$$

$\Delta\lambda$ being $\lambda_0 - \lambda_s$. On the other hand, the variable c_n is defined for the ULA as:

$$c_n = $$
$$2R_s[-\cos \delta_g \cos \phi_n \sin \Delta\lambda - \sin \delta_g \sin \phi_0 \cos \phi_n \cos \Delta\lambda$$
$$+ \cos \phi_0 \sin \delta_g \sin \phi_n]. \quad (18)$$

While for the UCA this variable is defined as:

$$c_{n,m} = $$
$$2R_s(\cos \alpha_m \cos \phi_s \sin \Delta\lambda + \sin \alpha_m \sin \phi_g \cos \phi_s \cos \Delta\lambda$$
$$- \cos \phi_g \sin \alpha_m \sin \phi_s) + 2d_s \cos(\alpha_m - \delta_s). \quad (19)$$

Utilizing first-degree approximations for $r_{n,m}$ and (13),for detailed development, please refer to [4], [14], the conditions are as follows, in the ULA architecture:

$$\frac{d_g}{2s_1 s_2}[c_1 s_2 - c_2 s_1 + 2d_s \cos \Delta\delta(s_2 - s_1)] = \zeta \cdot \frac{c_0}{Mf_c}, \quad (20)$$

and for the UCA scenario:

$$\frac{D}{4s_1 s_2}[(c_{1,k} + c_{1,l})s_2 - (c_{2,k} + c_{2,l})s_1] = \zeta(k \ominus l)\frac{c_0}{Mf_c}. \quad (21)$$

It is now explicitly evident that the optimum capacity depends on the space segment dynamics. It is worth noting that the optimum for the ULA does not depend on the variables k and l, unlike the UCA. Furthermore, in the case of the ULA, the expression contains a term directly influenced by the constant projection parameter $\cos \Delta\delta$. In the UCA case however, the projection term varies for each element $\cos(\alpha_m - \delta_s)$. The implications of this projection will be further discussed in the design trade-offs section.

IV. COMPARISON FRAMEWORK

In this section, we propose a comparison parameter allowing to assess the overall array performance across all potential trajectories in the FoV, as illustrated in Fig. 3b.

A. Size comparison

First, for the sake of fairness between the geometries, the comparable array dimensions are those enclosed by the same surface Ω (Fig. 1). The surface diameter is used to characterize the size of the ground array:

$$\Omega_d = \begin{cases} (M-1)d_g & \text{for ULA} \\ D & \text{for UCA} \end{cases} \quad (22)$$

B. Normalized Mean Channel Condition Number in FoV

The channel matrix, and consequently the eigenvalues γ_i of the $\mathbf{V}$ matrix, encapsulate two phenomena. The first is linked to the propagation distance in $a(\beta_0)$, which affect similarly both arrays. The second phenomenon is associated to the specific geometry. In the $2 \times M$ MIMO architecture, the two eigenvalues are $\gamma_{+,-} = |a(\beta_0)|^2 M \pm |a(\beta_0)|^2 \sqrt{\psi_{n,m}}$, where

$$\psi_{n,m} = \sum_{k=1}^{M} \sum_{l=1}^{M} \exp\left(j\frac{2\pi}{\lambda}[(r_{1,k} - r_{2,k}) - (r_{1,l} - r_{2,l})]\right). \quad (23)$$

Since our focus here is on the array geometry rather than the link budget, which is heavily determined by the antenna implementation, we analyze the condition number of the $\mathbf{V}$ matrix. The condition number κ is given by:

$$\kappa(\mathbf{V}) = \frac{\gamma_+}{\gamma_-} = \frac{M + \sqrt{\psi_{n,m}}}{M - \sqrt{\psi_{n,m}}}. \quad (24)$$

This approach allows us to isolate the impact of the array geometry on the MIMO channel quality. The role of the antenna design on the link budget will be the focus of future research works. There, the optimal trade-off between

achievable data rates and antenna hardware complexity will be thoroughly investigated. Given the substantial MIMO spatial multiplexing gain, one envisioned course of action is to accept a reduction in individual antenna gains or the utilization of lower complexity equipment (e.g. antennas with wider beams to simplify satellite tracking).

To assess the performance of κ, over all possible crossings of the two orbital segments (Fig. 3b), we employ the averaging expression (25) in terms of κ^{-1}. The use of the inverse of the condition number prevents infinite values when the keyhole capacity is observed ($\gamma_- = 0$). Finally, the expression is normalized to range between 0, when all points are at keyhole capacity, up to 1 in the optimum scenario, where the κ^{-1} value of both segments is 1:

$$\Upsilon = \frac{\iint_{FoV}(\kappa^{-1}_{ascending} + \kappa^{-1}_{descending})dS}{\iint_{FoV}(1_{ascending} + 1_{descending})dS}. \quad (25)$$

The expression for Υ can be solved numerically, and the geometry performance can be optimized by maximizing it.

V. Numerical Simulation and Design Trade-Offs

In order to evaluate the behavior of each array configuration, we compute both of the channel eigenvalues. For each point of the discretized gateway FoV, both $\gamma_{+/-}$ are averaged throughout the Υ indicator for both orbital segments (Fig. 3a). In the following analysis, we examine a feeder link uplink scenario for a LEO orbit. This scenario resembles those used by Starlink in their first generation [15], with the on-board antennas aligned with the orbit. The detailed simulation parameters are summarized in Table I, unless otherwise specified.

TABLE I: Simulated constellation parameters

Parameter	Value
Carrier frequency	30 GHz
Altitude	600 km
Orbit inclination	70°
Space Antennas separation	2.5 m
Minimum Elevation	20°

A. Array size and orientation

The first relation to analyze is the dependency on the array orientation and the array size. Fig. 5 and Fig. 6 show a heat map of 3 and 6 elements ULA and UCA. The benefits of doubling the number of elements in the array are clear, resulting in a significant 40% Υ increase in both 6-element arrays. It is important to notice that this increase is attributable to the geometrical arrangement and not due to a power gain, as the condition number is independent of the link budget.

Both of the array types exhibit an area of low Υ values, consistently below 0.1, regardless of the orientation δ_g. This region occurs for the ULA when $\frac{\Omega_d(s_1-s_2)R_s}{(M-1)s_1 s_2} << \frac{c_0}{Mf_c}$ and in the UCA when $\frac{\Omega_d(s_1-s_2)R_s}{s_1 s_2} << \frac{c_0}{Mf_c}$. Within this area, spatial multiplexing is not feasible as the channel experiences mostly keyhole capacity. At these distances, the use of distributed
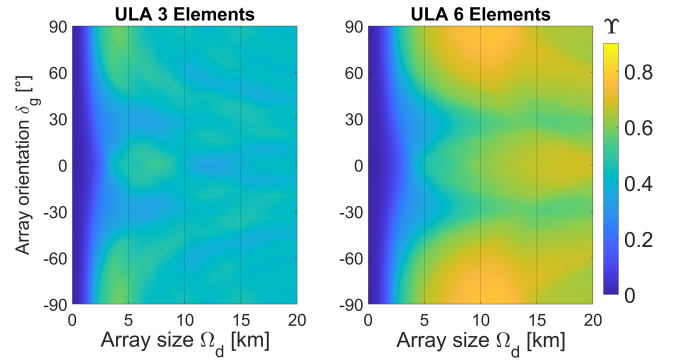

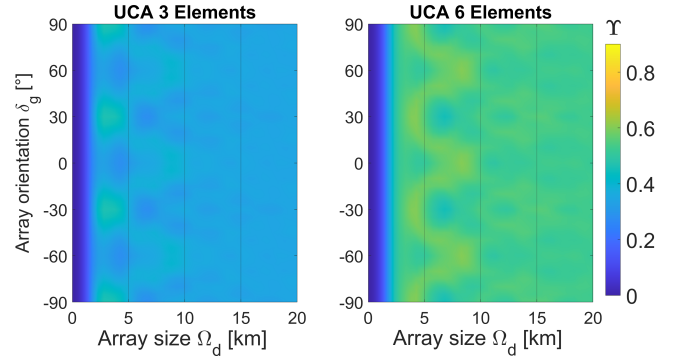Fig. 5: ULA channel performance as a function of the array orientation δ_g

Fig. 6: UCA channel performance as a function of the array orientation δ_g

systems can be considered for beam-forming purposes, with the aim of enhancing the communication CNR.

The highest Υ is obtained for the 6-element ULA, with $\Upsilon = 0.78$ under the optimal $\delta_g = \pm 90°$ and $\Omega_d = 10$ km. However, Υ for the UCA peaks 20% lower at 0.6, but remains stable to changes in size or orientation, unlike the ULA. Intuitively, this behavior is attributed to the ULA projection term of Section III-C, which achieves its maximum at the same angle δ_g for all the array antennas. In contrast, the UCA element-dependent projection results in a lower Υ.

B. Array design depending on the Constellation Altitude

For this section, the parameters δ_g and M are fixed to 90° (south to north orientation) and 6, respectively. Fig. 7 illustrates the influence of the altitude and array size in Υ.

The zone of no spatial multiplexing widens at higher altitudes, consistent with our previous analysis, as the term $s_1 s_2$ increases faster than R_s. As expected, this region is notably shorter for the UCA. Furthermore, the UCA distribution reaches its peak Υ at smaller size Ω_d when compared to the ULA array, allowing for compact designs if required. Additionally, the ULA array exhibits a broader altitude stability range than the UCA, making it suitable for multi-shell constellations.
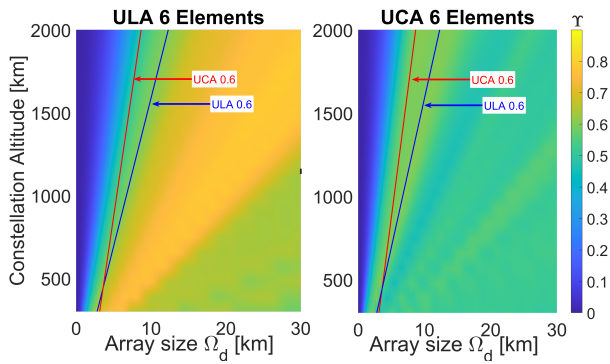
Fig. 7: Size vs Altitude trade-offs. Trend lines show the smaller arrays to achieve 0.6.
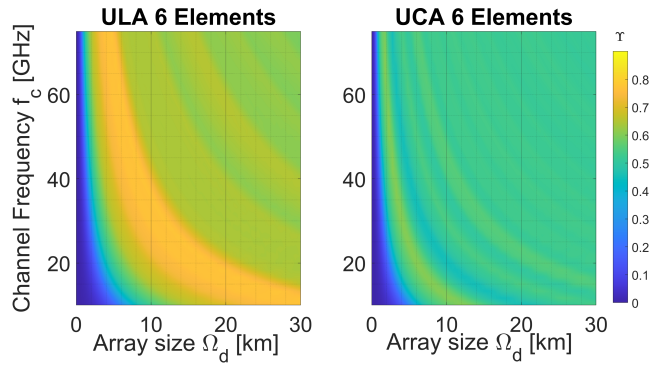

Fig. 8: Frequency dependency of the Arrays performances.

C. Frequency stability of the array

Finally, in this subsection we analyze the performance indicator for different carrier frequencies. Fig. 8 presents the frequency dependency of Υ for various array sizes.

For both ULA and UCA arrays covering the Ka-band, there is a design trade-off in Υ to be made between uplink and downlink frequencies. For instance, consider a Ka uplink-optimized ULA, designed to operate between 27.5 and 31 GHz with a size of $\Omega_d = 10$ km. However, this particular architecture experiences a 10% reduction in Υ for the downlink frequencies in the range 17.7 to 21.2 GHz. If we define an array bandwidth covering 90% of the maximum Υ, this Ka ULA would cover around 20 GHz, from 17.7 GHz to 38 GHz.

Now consider another ULA design, this time optimized to operate around 60 GHz with $\Omega_d = 5$ km. In this case, the available bandwidth doubles, extending from 38 to 78 GHz. These analyzed array geometries, ensure favorable link conditions over broader ranges when designed for higher operational frequencies.

VI. CONCLUSION

This paper conducted a comparative study of the applicability of ULA and UCA arrays for MIMO uplinks in NGSO communications. We derived the instantaneous optimum capacity conditions within the dynamic NGSO context for each configuration. For the subsequent performance comparison across the Field of View, we introduced a novel performance indicator based on the mean inverse condition number. Our numerical results, considering a typical constellation scenario, consistently favored the optimized ULA configuration over the UCA counterpart, demonstrating a 20% gap in channel matrix quality. Additionally, the ULA array exhibits multi-shell capabilities and stability over a large frequency range, extending up to 40 GHz, further emphasizing its potential for NGSO MIMO uplink applications.

REFERENCES

[1] I. del Portillo, B. Cameron, and E. Crawley, "Ground Segment Architectures for Large LEO Constellations with Feeder Links in EHF-bands," 2018.

[2] V. M. Baeza, F. Ortiz, E. Lagunas, T. S. Abdu, and S. Chatzinotas, "Multi-Criteria Ground Segment Dimensioning for Non-Geostationary Satellite Constellations," *2023 Joint European Conference on Networks and Communications and 6G Summit, EuCNC/6G Summit 2023*, pp. 252–257, 2023.

[3] M. Kan, "Starlink speeds continue to fall in the US, Canada amid network congestion," Nov 2022. [Online]. Available: https://uk.pcmag.com/networking/144109/starlink-speeds-continue-to-fall-in-the-us-canada-amid-network-congestion

[4] R. T. Schwarz, T. Delamotte, K.-U. Storek, and A. Knopp, "MIMO Applications for Multibeam Satellites," *IEEE Transactions on Broadcasting*, vol. 65, no. 4, pp. 664–681, 2019.

[5] A. Guidotti, C. Sacchi, and A. Vanelli-Coralli, "Feeder Link Precoding for Future Broadcasting Services," *IEEE Transactions on Aerospace and Electronic Systems*, vol. 58, no. 4, pp. 3126–3146, 2022.

[6] T. Delamotte and A. Knopp, "Smart Diversity through MIMO Satellite Q/V-Band Feeder Links," *IEEE Transactions on Aerospace and Electronic Systems*, vol. 56, pp. 285–300, 2 2020.

[7] L. Li, T. Chen, W. Wang, X. Song, L. You, and X. Gao, "LoS MIMO transmission for LEO satellite communication systems," *China Communications*, vol. 19, pp. 180–193, 10 2022.

[8] D. Goto, H. Shibayama, F. Yamashita, and T. Yamazato, "LEO-MIMO Satellite Systems for High Capacity Transmission," in *2018 IEEE Global Communications Conference (GLOBECOM)*, 2018, pp. 1–6.

[9] R. Richter, I. Bergel, Y. Noam, and E. Zehavi, "Downlink Cooperative MIMO in LEO Satellites," *IEEE Access*, vol. 8, pp. 213 866–213 881, 2020.

[10] Federal Communications Commission, "FCC report - Radio Station Authorization." [Online]. Available: https://fcc.report/IBFS/SES-LIC-20230427-00924

[11] S. Hong, W. Shin, and J. Lee, "Doppler Analysis and Compensation for Distributed LEO-MIMO Satellite Communications," in *2022 27th Asia Pacific Conference on Communications (APCC)*, 2022, pp. 629–630.

[12] E. Mollaymeri, T. Delamotte, and A. Knopp, "Time and phase alignment of distributed gateways: Theoretical analysis and experimental demonstration," *International Journal of Satellite Communications and Networking*, 2023. [Online]. Available: https://onlinelibrary.wiley.com/doi/abs/10.1002/sat.1500

[13] I. Telatar, "Capacity of Multi-antenna Gaussian Channels," *European Transactions on Telecommunications*, 1999.

[14] V. Dantona, R. Schwarz, A. Knopp, and B. Lankl, "Uniform Circular Arrays: the Key to Optimum Channel Capacity in Mobile MIMO Satellite Links," *5th Advanced Satellite Multimedia Systems Conference and the 11th Signal Processing for Space Communications Workshop*, 2010.

[15] Federal Communications Commission, "FCC.report - SAT-MOD-20200417-00037, Attachment Technical Attach." [Online]. Available: https://fcc.report/IBFS/SAT-MOD-20200417-00037/2274316